# On the Conflicting Pictures of Magnetism for the Frustrated Triangular Lattice Antiferromagnet $CuFeO_2$

Myung-Hwan Whangbo* and Dadi Dai

*Department of Chemistry, North Carolina State University, Raleigh, North Carolina 27695-8204*

Kwang-Soon Lee

*Department of Chemistry, The Catholic University of Korea, Bucheon, Gyeonggi-Do, South Korea 422-743*

Reinhard K. Kremer

*Max-Planck-Institut für Festkörperforschung, Heisenbergstrasse 1, D-70569 Stuttgart, Germany*

*Received November 29, 2005. Revised Manuscript Received January 17, 2006*

The magnetic structures of the triangular lattice antiferromagnet $CuFeO_2$ below 14 K are described by an Ising model despite the fact that its high-spin $Fe^{3+}$ ($d^5$) ions ($S = 5/2$, $L = 0$) cannot have a uniaxial magnetic moment. To resolve this puzzling picture of magnetism, we estimated the relative strengths of various spin-exchange interactions of $CuFeO_2$ by performing a spin dimer analysis and then determined the relative stabilities of a number of ordered spin states of $CuFeO_2$. Our calculations show that, in terms of a Heisenberg model, the noncollinear 120° spin arrangement predicted for a triangular lattice antiferromagnet is more stable than the collinear four-sublattice antiferromagnetic structure observed for $CuFeO_2$ below 11 K. To find a probable cause for stabilizing the collinear spin alignment along the *c* axis below 14 K, we considered the defect ions $Fe^{2+}$ and $Cu^{2+}$ of the $CuFeO_2$ lattice created by oxygen deficiency and oxygen excess, respectively. Our electronic structure analysis suggests that these defect ions generate uniaxial magnetic moments along the *c* axis and hence induce the surrounding $Fe^{3+}$ ions to orient their moments along the *c* axis.

## 1. Introduction

The crystal structure of the delafossite $CuFeO_2$ consists of $FeO_2$ layers that are made of edge-sharing $FeO_6$ octahedra (Figure 1a); these layers are bridged by Cu atoms to form linear O−Cu−O dumbbells perpendicular to the layers (Figure 1b).[1] Mössbauer studies[2] of $CuFeO_2$ show its Fe atoms are present as $Fe^{3+}$ ($d^5$) ions, and hence the Cu atoms are present as diamagnetic $Cu^+$ ($d^{10}$) ions. The studies also show that $CuFeO_2$ becomes antiferromagnetically ordered below 14 K. Furthermore, the magnetic susceptibility studies[3] of $CuFeO_2$ showed that the $Fe^{3+}$ ($d^5$) ions are in a high-spin state, and the antiferromagnetic coupling between the $Fe^{3+}$ ions is dominant within rather than between $FeO_2$ layers. The triangular lattice of the magnetic $Fe^{3+}$ ions in each $FeO_2$ layer is an archetypal spin lattice that causes geometric spin frustration.[4] The frustrated nature of the magnetic properties of $CuFeO_2$ have been the subject of a number of studies.[5−11]

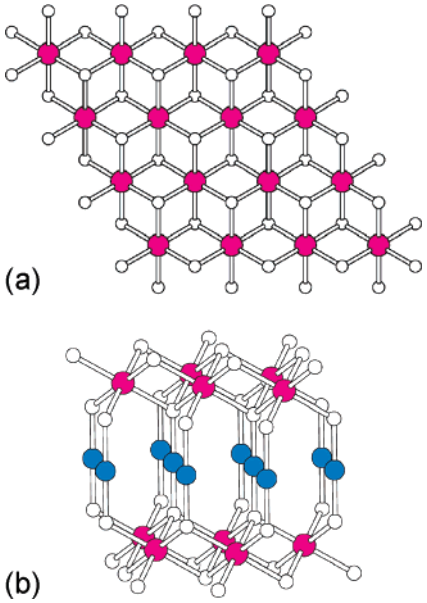


**Figure 1.** (a) Perspective view of an isolated $FeO_2$ layer made of edge-sharing $FeO_6$ octahedra. (b) Perspective view of two adjacent $FeO_2$ layers linked by O−Cu−O bridges. The Fe, Cu, and O atoms are indicated by red, blue, and white circles.

When the temperature is lowered, $CuFeO_2$ undergoes a phase transition from a paramagnetic state to an incommensurately

(1) (a) Prewitt, C. T.; Shannon, R. D.; Rogers, D. B. *Inorg. Chem.* **1971**, *10*, 719. (b) Pabst, A. *Am. Mineral.* **1946**, *31*, 539. (c) Soller, W.; Thompson, A. J. *Phys. Rev.* **1935**, *47*, 644.

(2) (a) Muir, A. H., Jr.; Wiedersich, H. *J. Phys. Chem. Solids* **1967**, *28*, 65. (b) Muir, A. H., Jr.; Grant, R. W.; Wiedersich, H. *Proceedings of the Conference on the Application of Mössbauer Effect*, Tihany, Hungary, 1969.

(3) (a) Doumerc, J.-P.; Wichainchai, A.; Ammar, A.; Pouchard, M.; Hagenmuller, P. *Mater. Res. Bull.* **1986**, *21*, 745. (b) El Ataoui, K.; Doumerc, J.-P.; Ammar, A.; Fournès, L.; Wattiaux, A.; Grenier, J.-C.; Pouchard, M. *J. Alloys Compd.* **2004**, *368*, 79.

(4) (a) Greedan, J. E. *J. Mater. Chem.* **2001**, *11*, 37. (b) Dai, D.; Whangbo, M.-H. *J. Chem. Phys.* **2004**, *121*, 672.

(5) Mitsuda, S.; Yoshizawa, H.; Yaguchi, N.; Mekata, M. *J. Phys. Soc. Jpn.* **1991**, *60*, 1885.

10.1021/cm052634g CCC: $33.50 
Published on Web 02/08/2006

ordered antiferromagnetic (AF) state at $T_{N1} = 14$ K and then to a collinear four-sublattice AF state at $T_{N2} = 11$ K.[6,7] There is a thermal hysteresis in the 11 K transition, which indicates the phase transition is first-order. When placed in a magnetic field at a temperature below $T_{N2}$, $CuFeO_2$ undergoes several phase transitions if the field is parallel to the *c* axis (i.e., perpendicular to the $FeO_2$ layer) but one phase transition if the field is perpendicular to the *c* axis.[8] The occurrence of such ordered magnetic structures has been explained in terms of a two-dimensional (2D) Ising model.[6,8−10] As recently pointed out by Petrenko et al.,[11] however, the magnetic properties of $CuFeO_2$ above $T_{N1}$ should be explained by a Heisenberg rather than an Ising model.

There are many compelling reasons why an Ising model is not self-consistent for $CuFeO_2$.[11] This model predicts an anisotropic magnetic susceptibility above a three-dimensional (3D) ordering temperature $T_{N1}$, but the magnetic susceptibility measured for single crystals of $CuFeO_2$ is rather isotropic above $T_{N1}$.[8,11−13] An Ising model is relevant for a magnetic system in which each of its spin sites has a uniaxial magnetic moment. However, a high-spin $Fe^{3+}$ ion ($S = 5/2$, $L = 0$) in an octahedral environment cannot provide a uniaxial magnetic moment,[14] because its orbital angular momentum is zero. The ordered spin arrangement of a triangular lattice antiferromagnet (TLA) predicted from a Heisenberg model is the (1/3, 1/3) superstructure (Figure 2a) in which each triangular plaquette has a noncollinear 120° spin arrangement.[4] Indeed, this ordered spin structure is observed for the $CrO_2$ layers of the delafossites $LiCrO_2$ and $CuCrO_2$.[15] Therefore, it is puzzling why each $FeO_2$ layer of $CuFeO_2$ below $T_{N2}$ does not adopt this spin arrangement expected for a TLA but instead adopts the collinear four-sublattice AF arrangement (Figure 2b)[6] in which the magnetic moment at each $Fe^{3+}$ site is parallel to the *c* axis. Recent attempts to explain the unusual magnetic properties of $CuFeO_2$ are made on the basis of lattice distortions[16] and correlated magnetoelectric/magnetoelastic phenomena.[17] An important clue for resolving the conflicting pictures of magnetism for $CuFeO_2$ might lie in the observation that the stability of the collinear four-sublattice AF structure is sensitively affected by a small amount of point defects.[12,18] Namely, the collinear four-sublattice AF structure of $CuFeO_2$ disappears when a small number of nonmagnetic $Al^{3+}$ ions are substituted for $Fe^{3+}$ (i.e., 2%).[18] The collinear four-sublattice AF structure is maintained in nonstoichiometric $CuFeO_{2+\delta}$ single crystals with either oxygen deficiency ($\delta < 0$) or oxygen excess ($\delta > 0$), but the phase-transition temperature $T_{N2}$ is increased by oxygen deficiency, whereas it is decreased by oxygen excess.[12] The oxygen deficiency generates $Fe^{2+}$ ions, and the oxygen excess generates $Cu^{2+}$ ions. It is crucial to understand how the presence of such defect ions can influence the stability of the collinear four-sublattice AF structure.

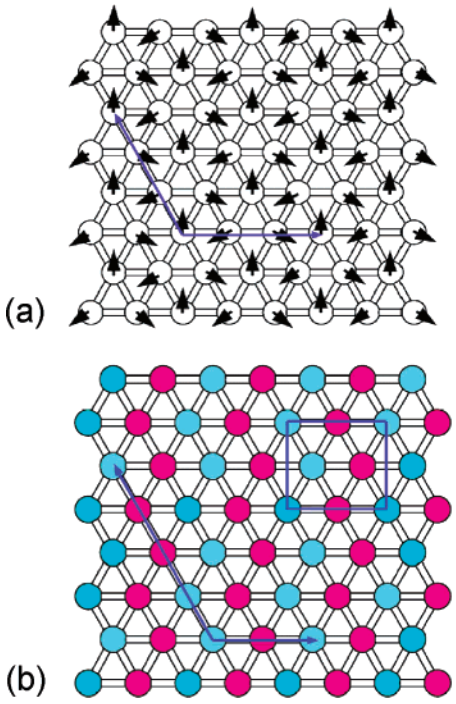


**Figure 2.** Magnetic superstructures of an $FeO_2$ layer: (a) noncollinear 120° magnetic structure, i.e., (1/3, 1/3) magnetic superstructure, where the small arrow at each spin site represents the spin moment. (b) Collinear four-sublattice antiferromagnetic structure, i.e., (1/2, 1/4) magnetic superstructure, where the spin moments parallel and antiparallel to the *c* axis are distinguished by circles with two different colors and the rectangular box represents the smallest unit cell.

In the present work, we probe why an Ising model is required for explaining the ordered magnetic structures of $CuFeO_2$ below $T_{N1}$ despite the fact that this model is not supported on the basis of electronic structure considerations. Our work is organized as follows: In section 2, we estimate the relative strengths of various spin-exchange parameters of $CuFeO_2$ that are consistent with its electronic structure. Using these parameters, we calculate in section 3 the total spin-exchange interaction energies of various 3D ordered-spin arrangements of $CuFeO_2$ to find that the collinear four-sublattice AF structure of an isolated $FeO_2$ layer is less stable than the (1/3, 1/3) superstructure in terms of a Heisenberg model. In section 4, we examine whether the defect ions $Fe^{2+}$ and $Cu^{2+}$ of the $CuFeO_2$ lattice generated by oxygen nonstoichiometry can provide a driving force for the $Fe^{3+}$ ions to orient their moments along the *c* axis, thereby stabilizing the collinear four-sublattice AF structure below $T_{N2}$. The important results of our work are summarized in section 5.

(6) Mekata, M.; Yaguchi, N.; Takagi, T.; Sugino, T.; Mitsuda, S.; Yoshizawa, H.; Hosoito, N.; Shinjo, T. *J. Phys. Soc. Jpn.* **1993**, *62*, 4474.
(7) Takeda, K.; Miyake, K.; Hitaka, M.; Kawae, T.; Yaguchi, N.; Mekata, M. *J. Phys. Soc. Jpn.* **1994**, *63*, 2017.
(8) Ajiro, Y.; Asano, T.; Takagi, T.; Mekata, M.; Agura-Katori, H.; Goto, T. *Physica B* **1994**, *201*, 71.
(9) Takagi, T.; Mekata, M. *J. Phys. Soc. Jpn.* **1995**, *64*, 4609.
(10) Petrenko, O. A.; Balakrisnan, G.; Lees, M. R.; Paul, D. McK.; Hoser, A. *Phys. Rev. B* **2000**, *62*, 8983.
(11) Petrenko, O. A.; Lees, M. R.; Balakrisnan, G.; de Brion, S.; Chouteau, G. *J. Phys.: Condens. Matter* **2005**, *17*, 2741.
(12) Hasegawa, M.; Batrashevich, M. I.; Zhao, T.-R.; Takei, H.; Goto, T. *Phys. Rev. B* **2001**, *63*, 184437.
(13) Terada, N.; Mitsuda, S.; Suzuki, S.; Kawasaki, T.; Fukuda, M.; Nagao, T.; Aruga-Katori, H. *J. Phys. Soc. Jpn.* **2004**, *73*, 1442.
(14) Dai, D.; Whangbo, M.-H. *Inorg. Chem.* **2005**, *44*, 4407.
(15) Collins, M. F.; Petrenko, O. A. *Can. J. Phys.* **1997**, *75*, 605.
(16) Terada, N.; Mitsuda, S.; Ohsumi, H.; Tajima, K. *J. Phys. Soc. Jpn.* In press.
(17) Kimura, T.; Lashley, J. C.; Ramirez, A. P. arXiv: cond-mat/0510701, http://xxx.lanl.gov/pdf/cond-mat/0510701.
(18) Terada, N.; Mitsuda, S.; Prokes, K.; Suzuki, O.; Kitazawa, H.; Aruga-Katori, H. *Phys. Rev. B* **2004**, *70*, 174412.

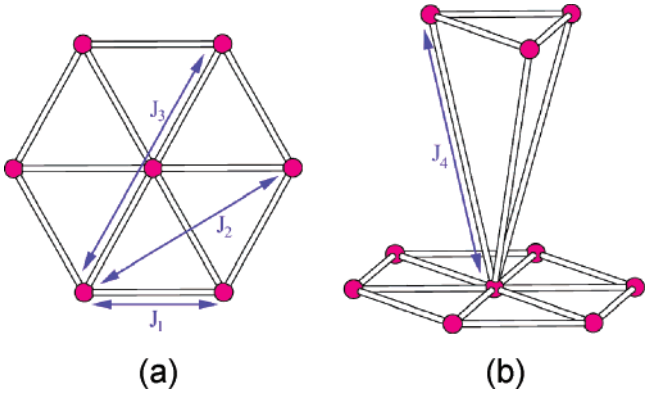


**Figure 3.** (a) Spin-exchange paths $J_1$, $J_2$, and $J_3$ within an $FeO_2$ layer. (b) Spin-exchange path $J_4$ between adjacent $FeO_2$ layers.

**Table 1. Geometrical Parameters and $\langle(\Delta e)^2\rangle$ Values Associated with the Spin-Exchange Interactions $J_1$, $J_2$, $J_3$, and $J_4$ of $CuFeO_2$**

| interaction | geometrical parameters[a] | $\langle(\Delta e)^2\rangle$ (meV$^2$) |
|---|---|---|
| $J_1$ | Fe−O−Fe<br>Fe···Fe = 3.035 Å<br>∠Fe−O−Fe = 96.6° | 1570 (1.00)[b] |
| $J_2$ | Fe−O···O−Fe<br>Fe···Fe = 5.257 Å<br>O···O = 2.706 Å<br>∠Fe−O···O = 99.9° | 32 (0.020) |
| $J_3$ | Fe−O···O−Fe<br>Fe···Fe = 6.070 Å<br>O···O = 3.035 Å<br>∠Fe−O···O = 138.3° | 50 (0.032) |
| $J_4$ | Fe−O−Cu−O−Fe<br>Fe···Fe = 5.984 Å<br>O−Cu = 1.830 Å<br>∠Fe−O−Cu = 120.5°<br>∠O−Cu−O = 180° | 36 (0.023) |

[a] All Fe−O = 2.033 Å. [b] The numbers in parentheses give the relative tendency for antiferromagnetic coupling.

## 2. Spin Dimer Analysis

In describing the magnetic properties of $CuFeO_2$ in terms of an Ising model, we have employed three intralayer spin-exchange interactions $J_1$, $J_2$, and $J_3$ (Figure 3a) while neglecting the interlayer spin-exchange interaction $J_4$ (Figure 3b).[6,9] We estimate the relative strengths of these interactions by performing spin dimer analysis on the basis of extended Hückel tight-binding (EHTB) electronic structure calculations.[19] The spin dimers (i.e., the structural units made of two $Fe^{3+}$ ions plus the oxygen atoms in their first coordinate spheres) leading to the $J_1$, $J_2$, $J_3$, and $J_4$ interaction are depicted in Figure 4. These interactions are of the superexchange (SE) type involving Fe−O−Fe paths (i.e., $J_1$), the super-superexchange (SSE) type involving Fe−O···O−Fe paths within each $FeO_2$ layer (i.e., $J_2$ and $J_3$), and the SSE type involving Fe−O−Cu−O−Fe paths between adjacent $FeO_2$ layers (i.e., $J_4$). The important structural parameters describing these spin-exchange paths are listed in Table 1.

The spin-exchange parameter $J$ is written as $J = J_F + J_{AF}$, where the ferromagnetic term $J_F$ is positive and the antiferromagnetic term $J_{AF}$ is negative. In general, $J_F$ is very small, so that the trends in the $J$ values are well-approximated by those in the corresponding $J_{AF}$ values.[19] In spin dimer analysis completed on the basis of EHTB calculations, the strength of an antiferromagnetic interaction between two spin sites is estimated by considering the antiferromagnetic spin exchange parameter $J_{AF}$[19]

$$J_{AF} \approx -\frac{\langle(\Delta e)^2\rangle}{U_{eff}} \quad (1)$$

where $U_{eff}$ is the effective on-site repulsion that is essentially a constant for a given compound. The $\langle(\Delta e)^2\rangle$ term is calculated by performing tight-binding electronic structure calculations for a spin dimer. Each $Fe^{3+}$ ion of $CuFeO_2$ has five singly occupied d-block levels $\phi_\mu$ ($\mu = 1-5$), i.e., five magnetic orbitals. Thus, the $\langle(\Delta e)^2\rangle$ term is given by

$$\langle(\Delta e)^2\rangle \approx \frac{1}{5^2}\sum_{\mu=1}^{5}(\Delta e_{\mu\mu})^2 \quad (2)$$

where $\Delta e_{\mu\mu}$ is the energy split that results when two magnetic orbitals $\phi_\mu$ ($\mu = 1-5$) on adjacent spin sites interact (Figure 5). Because $U_{eff}$ is essentially a constant for a given compound, the trend in the $J_{AF}$ values is determined by that in the corresponding $\langle(\Delta e)^2\rangle$ values. For the spin-exchange interactions $J_1-J_4$ of $CuFeO_2$, we calculate the corresponding $\langle(\Delta e)^2\rangle$ values using the spin dimers shown in Figure 4. The atomic parameters of Fe, Cu, and O used for our EHTB calculations[20] are summarized in Table 2. Table 1 summarizes the calculated $\langle(\Delta e)^2\rangle$ values together with their relative values.

Table 1 reveals that the SE interaction $J_1$ is the strongest AF spin-exchange interaction in $CuFeO_2$. The intralayer SSE interactions $J_2$ and $J_3$ are much weaker than $J_1$ (by factors of approximately 50 and 30, respectively). This is in sharp contrast to the observation[8] that, in order for the magnetic structures of $CuFeO_2$ below $T_{N2}$ and under magnetic field to be described in terms of a 2D Ising model, $J_2$ and $J_3$ should be quite strong (i.e., $J_2/J_1 = 0.5$ and $J_3/J_1 = 0.75$). Furthermore, the interlayer SSE interaction $J_4$ is not negligible but is comparable in strength to the intralayer SSE interactions $J_2$ and $J_3$. This is consistent with the finding that $CuFeO_2$ undergoes a 3D ordered magnetic structure below 14 K[7] and that neutron-scattering experiments show a significant dispersion along the interlayer direction.[21] For the interlayer interaction $J_4$, the two O−Cu−O bridges linking the two $FeO_6$ octahedra are crucial because our calculations lead to $\langle(\Delta e)^2\rangle = 0$ in the absence of the Cu atoms in the spin dimer (Figure 4d). The magnetic orbitals of the spin dimer show that the $3d_{z^2}$, $3d_{xz}$, and $3d_{yz}$ of the bridging Cu atoms (with the local $z$ axis taken along each O−Cu−O linkage) promote the interlayer SSE interaction $J_4$.

(19) For recent reviews, see: (a) Whangbo, M.-H.; Koo, H.-J.; Dai, D. *J. Solid State Chem.* **2003**, *176*, 417. (b) Whangbo, M.-H.; Dai, D.; Koo, H.-J. *Solid State Sci.* **2005**, *7*, 827.

(20) Our calculations were carried out by employing the SAMOA (Structure and Molecular Orbital Analyzer) program package: Dai, D.; Ren, J.; Liang, W.; Whangbo, M.-H. *SAMOA*; http://chvamw.chem.ncsu.edu/, 2002.

(21) Petrenko, O. A.; Fåk, B.; Bull, M. *ISIS Experimental Report RB;* 11734, 2001; ISIS: Chilton, U.K., 2001; www.isis.rl.ac.uk/isis2001/reports.

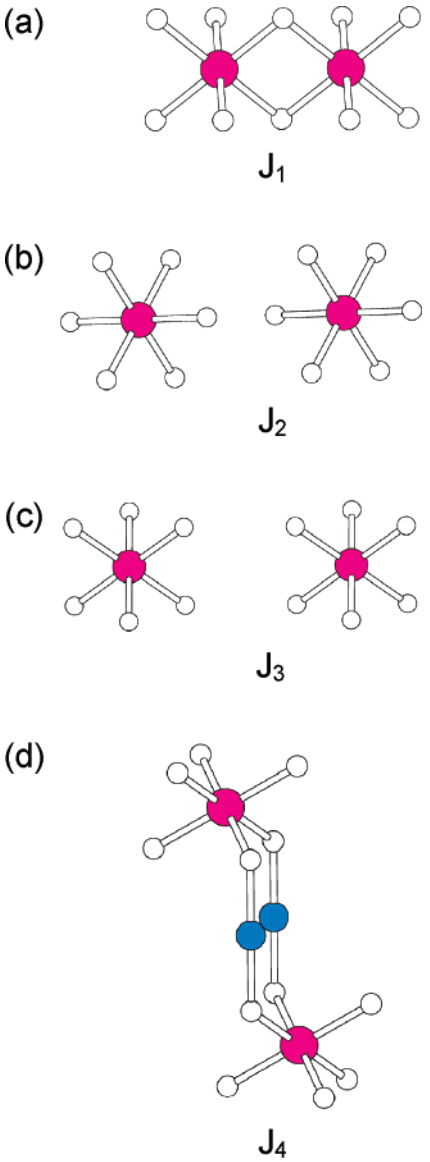


**Figure 4.** Spin dimers associated with the spin-exchange paths (a) $J_1$, (b) $J_2$, (c) $J_3$, and (d) $J_4$.

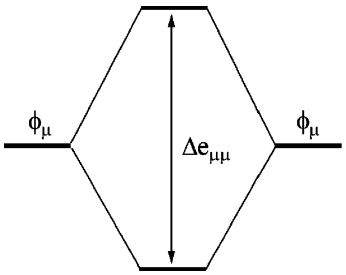


**Figure 5.** Interaction between two magnetic orbitals $\phi_\mu$ of a spin dimer leading to the energy split $\Delta e_{\mu\mu}$.

## 3. Ordered Magnetic Structure and Total Spin-Exchange Interaction Energy

In this section, we examine the total spin-exchange energies of various ordered magnetic structures of $CuFeO_2$ in terms of a Heisenberg model by using the Freiser method,[19b,22] in which the total spin-exchange energy of an ordered magnetic structure is calculated under the assumptions that spins adopt all possible directions in space (i.e., the classical spin approximation) and that the spin-exchange interactions are isotropic (i.e., a Heisenberg description). The classical spin approximation is best suited for a magnetic system made of spin-5/2 ions such as high-spin $Fe^{3+}$ ions.

(22) Freiser, M. J. *Phys. Rev.* **1961**, *123*, 2003.

**Table 2. Exponents $\zeta_i$ and Valence-Shell Ionization Potentials $H_{ii}$ of Slater-Type Orbitals $\chi_i$ Used for Extended Hückel Tight-binding Calculation**[a]

| atom | $\chi_i$ | $H_{ii}$ (eV) | $\zeta_i$ | $C^b$ | $\zeta'_i$ | $C'^b$ |
|---|---|---|---|---|---|---|
| Fe | 4s | −9.10 | 1.925 | 1.0 | | |
| Fe | 4p | −5.32 | 1.390 | 1.0 | | |
| Fe | 3d | −12.6 | 6.608 | 0.4038 | 2.618 | 0.7198 |
| Cu | 4s | −11.4 | 2.151 | 1.0 | | |
| Cu | 4p | −6.06 | 1.370 | 1.0 | | |
| Cu | 3d | −14.0 | 7.025 | 0.4473 | 3.004 | 0.6978 |
| O | 2s | −32.3 | 2.688 | 0.7076 | 1.675 | 0.3745 |
| O | 2p | −14.8 | 3.694 | 0.3322 | 1.659 | 0.7448 |

[a] The diagonal matrix element $H_{ii}$ is defined as $\langle\chi_i|H^{eff}|\chi_i\rangle$, where $H^{eff}$ is the effective Hamiltonian. In our calculations of the off-diagonal matrix elements $H^{eff} = \langle\chi_i|H^{eff}|\chi_j\rangle$, the weighted formula was used. [b] Contraction coefficients used in the double-$\zeta$ Slater-type orbital.

In a long-range ordered magnetic state $i$ of a magnetic system, the spin sites $\mu$ (= 1, 2, ..., $m$) of its unit cell located at the coordinate origin (i.e., the lattice vector $\mathbf{R} = 0$) have mean spins $\sigma_\mu{}^0$. At high temperatures, the spins are completely disordered so that $\sigma_\mu{}^0 = 0$ at all spin sites. As the temperature is lowered, an ordered spin arrangement may set in, thereby leading to nonzero $\sigma_\mu{}^0$. For a magnetic solid with repeat vectors **a**, **b**, and **c**, the ordered spin arrangement is described by the spin functions $\sigma_\mu(\mathbf{k})$

$$\sigma_\mu(\mathbf{k}) = \frac{1}{\sqrt{M}}\sum_{\mathbf{R}}\sigma_\mu{}^0 \exp(i\mathbf{k}\cdot\mathbf{R}) \quad (3)$$

where $M$ is the number of unit cells in the magnetic solid, **k** is the wave vector, and **R** is the direct lattice vector.[23] The ordered magnetic state $\psi_i(\mathbf{k})$ ($i = 1 - m$) is then expressed as a linear combination of the spin functions $\sigma_\mu(\mathbf{k})$

$$\psi_i(\mathbf{k}) = C_{1i}(\mathbf{k})\sigma_1(\mathbf{k}) + C_{2i}(\mathbf{k})\sigma_2(\mathbf{k}) + ... + C_{mi}(\mathbf{k})\sigma_m(\mathbf{k}) \quad (4)$$

To determine the energy $E_i(\mathbf{k})$ of the state $\psi_i(\mathbf{k})$ and the coefficients $C_{\mu i}(\mathbf{k})$ ($\mu = 1 - m$), one needs to evaluate the spin-exchange interaction energies $\xi_{\mu\nu}(\mathbf{k})$ between every two spin functions $\sigma_\mu(\mathbf{k})$ and $\sigma_\nu(\mathbf{k})$

$$\xi_{\mu\nu}(\mathbf{k}) = -\sum_{\mathbf{R}} J_{\mu\nu}(\mathbf{R}) \exp(i\mathbf{k}\cdot\mathbf{R}) \quad (5)$$

and diagonalize the resulting interaction matrix $\Xi(\mathbf{k})$

$$\Xi(\mathbf{k}) = \begin{bmatrix} \xi_{11}(\mathbf{k}) & \xi_{12}(\mathbf{k}) & ... & \xi_{1m}(\mathbf{k}) \\ \xi_{21}(\mathbf{k}) & \xi_{22}(\mathbf{k}) & ... & \xi_{2m}(\mathbf{k}) \\ ... & ... & ... & ... \\ \xi_{m1}(\mathbf{k}) & \xi_{m2}(\mathbf{k}) & ... & \xi_{mm}(\mathbf{k}) \end{bmatrix} \quad (6)$$

For a given set of spin-exchange parameters $J_{\mu\nu}$, one can determine the value of **k** that leads to the lowest energy $E_m$

(23) Given the lattice vector written as $\mathbf{R} = n_a\mathbf{a} + n_b\mathbf{b} + n_c\mathbf{c}$, where $n_a$, $n_b$, and $n_c$ are integers, and the wave vector **k** written as $\mathbf{k} = x_a\mathbf{a}^* + x_b\mathbf{b}^* + x_c\mathbf{c}^*$, where $\mathbf{a}^*$, $\mathbf{b}^*$, and $\mathbf{c}^*$ are the reciprocal vectors and $x_a$, $x_b$, and $x_c$ are dimensionless numbers, the exp(i**kR**) term of eq 3 becomes $\exp[i2\pi(x_a n_a + x_b n_b + x_c n_c)]$. For convenience, we denote **k** by showing only its dimensionless components, i.e., $\mathbf{k} = (x_a, x_b, x_c)$.

**Table 3. Pairs of Spin Sites ($\mu-\nu$) ($\mu$, $\nu$ = 1, 2, 3) Leading to the Spin-Exchange Spin interactions $J_1-J_4$**

| | ($\mu-\nu$) | |
|---|---|---|
| path | within a unit cell | between unit cells |
| $J_1$ | | (1−1), (2−2), (3−3) |
| $J_2$ | | (1−1), (2−2), (3−3) |
| $J_3$ | | (1−1), (2−2), (3−3) |
| $J_4$ | (1−2), (1−3) | (1−2), (1−3), (2−3) |

**Table 4. Nonzero Contributions to the Matrix Elements $\xi_{\mu\nu}(\mathbf{k})$ from the Various Spin-Exchange Paths**

| $\mu$ | $\nu$ | cell[a] | Fe···Fe (Å) | contribution to $\xi_{\mu\nu}(\mathbf{k})$ |
|---|---|---|---|---|
| 1 | 1[b] | [−2, −2, 0] | 6.070 | $-J_3 \exp(-i4\pi x_a - i4\pi x_b)$ |
| | | [2, 2, 0] | 6.070 | $-J_3 \exp(i4\pi x_a + i4\pi x_b)$ |
| | | [−2, −1, 0] | 5.257 | $-J_2 \exp(-i4\pi x_a - i2\pi x_b)$ |
| | | [2, 1, 0] | 5.257 | $-J_2 \exp(i4\pi x_a + i2\pi x_b)$ |
| | | [−2, 0, 0] | 6.070 | $-J_3 \exp(-i4\pi x_a)$ |
| | | [2, 0, 0] | 6.070 | $-J_3 \exp(i4\pi x_a)$ |
| | | [−1, −2, 0] | 5.257 | $-J_2 \exp(-i2\pi x_a - i4\pi x_b)$ |
| | | [1, 2, 0] | 5.257 | $-J_2 \exp(i2\pi x_a + i4\pi x_b)$ |
| | | [−1, −1, 0] | 3.035 | $-J_1 \exp(-i2\pi x_a - i2\pi x_b)$ |
| | | [1, 1, 0] | 3.035 | $-J_1 \exp(i2\pi x_a + i2\pi x_b)$ |
| | | [−1, 0, 0] | 3.035 | $-J_1 \exp(-i2\pi x_a)$ |
| | | [1, 0, 0] | 3.035 | $-J_1 \exp(i2\pi x_a)$ |
| | | [−1, 1, 0] | 5.257 | $-J_2 \exp(-i2\pi x_a + i2\pi x_b)$ |
| | | [1, −1, 0] | 5.257 | $-J_2 \exp(i2\pi x_a - i2\pi x_b)$ |
| | | [0, −2, 0] | 6.070 | $-J_3 \exp(-i4\pi x_b)$ |
| | | [0, 2, 0] | 6.070 | $-J_3 \exp(i4\pi x_b)$ |
| | | [0, −1, 0] | 3.035 | $-J_1 \exp(-i\pi x_b)$ |
| | | [0, 1, 0] | 3.035 | $-J_1 \exp(i\pi x_b)$ |
| 1 | 2 | [−1, −1, 0] | 5.984 | $-J_4 \exp(-i2\pi x_a - i2\pi x_b)$ |
| | | [−1, 0, 0] | 5.984 | $-J_4 \exp(-i2\pi x_a)$ |
| | | [0, 0, 0] | 5.984 | $-J_4$ |
| 1 | 3 | [−1, −1, 0] | 5.984 | $-J_4 \exp(-i2\pi x_a - i2\pi x_b)$ |
| | | [0, −1, 0] | 5.984 | $-J_4 \exp(-i2\pi x_b)$ |
| | | [0, 0, 0] | 5.984 | $-J_4$ |
| 2 | 3 | [0, −1, 1] | 5.984 | $-J_4 \exp(-i2\pi x_b + i2\pi x_c)$ |
| | | [0, 0, 1] | 5.984 | $-J_4 \exp(i2\pi x_c)$ |
| | | [1, 0, 1] | 5.984 | $-J_4 \exp(i2\pi x_a + i2\pi x_c)$ |

[a] The cell notation [$n_a$, $n_b$, $n_c$] indicates the unit cell position given by the direct lattice vector $\mathbf{R} = n_a\mathbf{a} + n_b\mathbf{b} + n_c\mathbf{c}$. It is used to show the contribution that occurs between the [0, 0, 0] and [$n_a$, $n_b$, $n_c$] cells. Thus, the notation [0, 0, 0] means the contribution that occurs within a unit cell. [b] The interactions between $\mu = 2$ and $\nu = 2$ and those between $\mu = 3$ and $\nu = 2$ are the same as those between $\mu = 1$ and $\nu = 1$.

of the bands $E_i(\mathbf{k})$ ($i$ = 1, 2, ..., $m$), which occurs from the lowest-lying band $E_1(\mathbf{k})$. If we denote this particular $\mathbf{k}$ point as $\boldsymbol{k}_m$, then the magnetic superstructure is described by $\psi_1(\mathbf{k}_m)$.

Because each unit cell of $CuFeO_2$ has three $Fe^{3+}$ ions, there are three spin-basis functions $\sigma_\mu(\mathbf{k})$ ($\mu$ = 1−3) to consider. The pairs ($\mu-\nu$) of the spin sites ($\mu$, $\nu$ = 1−3) leading to the spin-exchange interactions $J_1$, $J_2$, $J_3$, and $J_4$ are listed in Table 3, whereas the nonzero contributions to the matrix elements $\xi_{\mu\nu}(\mathbf{k})$ from the various spin-exchange paths of $CuFeO_2$ are summarized in Table 4. Thus the nonzero matrix elements $\xi_{\mu\nu}(\mathbf{k})$ are given by

$$\xi_{11}(\mathbf{k}) = \xi_{22}(\mathbf{k}) = \xi_{33}(\mathbf{k}) = -J_1\{2\cos[2\pi(x_a + x_b)] + 2\cos[2\pi x_a] + 2\cos[2\pi x_b]\} - J_2\{2\cos[2\pi(2x_a + x_b)] + 2\cos[2\pi(x_a + 2x_b)] + 2\cos[2\pi(x_a - x_b)]\} - J_3\{2\cos[4\pi(x_a + x_b)] + 2\cos[4\pi x_a] + 2\cos[4\pi x_b]\}$$

$$\xi_{12}(\mathbf{k}) = -J_4\{\exp[-i2\pi(x_a - x_b)] + \exp[-i2\pi x_a] + 1\}$$

$$\xi_{13}(\mathbf{k}) = -J_4\{\exp[-i2\pi(x_a - x_b)] + \exp[-i2\pi x_b] + 1\}$$

$$\xi_{23}(\mathbf{k}) = -J_4\{\exp[i2\pi(x_a + x_c)] + \exp[i2\pi(-x_b + x_c)] + \exp[i2\pi x_c]\} \quad (7)$$

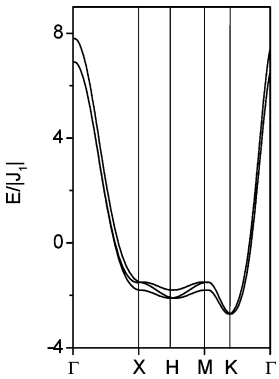


**Figure 6.** $E_i(\mathbf{k})$ vs $\mathbf{k}$ plots calculated for $J_2/J_1 = J_3/J_1 = J_4/J_1 = 0.1$, where $\Gamma$ = (0, 0, 0), X = (1/2, 0, 0), M = (1/2, 1/2, 0), H = (1/2, 1/4, 0), and K = (1/3, 1/3, 0).

**Table 5. Total Spin-Exchange Energies of a Single $FeO_2$ Layer for the Ordered Spin Arrangements Described by Some Special Positions in the Brillouin Zone**

| wave vector | energy per spin site |
|---|---|
| $\Gamma$ = (0, 0, 0) | $-3J_1 - 3J_2 - 3J_3$ |
| X = (1/2, 0, 0) | $J_1 + J_2 - 3J_3$ |
| M = (1/2, 1/2, 0) | $J_1 + J_2 - 3J_3$ |
| H = (1/2, 1/4, 0) | $J_1 - J_2 + J_3$ |
| K = (1/3, 1/3, 0) | $3J_1/2 - 3J_2/2 + 3J_3/2$ |

Figure 6 shows a representative $E_i(\mathbf{k})$ vs $\mathbf{k}$ plot calculated for the wave vector region $\Gamma-X-M-\Gamma$, where $\Gamma$ = (0, 0, 0), X = (1/2, 0, 0), and M = (1/2, 1/2, 0). For this particular plot, we used $J_2/J_1 = J_3/J_1 = J_4/J_1 = 0.1$ to accentuate the characteristic features of the $E_i(\mathbf{k})$ vs $\mathbf{k}$ plot. The three bands should be closer together than they appear in the plot because the values of $J_2/J_1$, $J_3/J_1$, and $J_4/J_1$ should be smaller than 0.1, according to our estimates in the previous section. The ordered spin arrangements of an isolated $FeO_2$ layer given by the wave vectors $\Gamma$, X, and M are shown in Figure 7. Along the line X−M, the energy minimum occurs at H = (1/2, 1/4, 0), which gives rise to the four-sublattice AF structure (Figure 2b) in each $FeO_2$ layer. Along the M−$\Gamma$ line, the minimum energy occurs at K = (1/3, 1/3, 0), which leads to the (1/3, 1/3) superstructure that has the noncollinear three-sublattice 120° arrangement (Figure 2a) in each $FeO_2$ layer. It is noticed that with the Heisenberg description, the (1/3, 1/3) superstructure is considerably more stable than the (1/2, 1/4) superstructure.

To probe the primary spin-exchange interactions responsible for the formation of the (1/2, 1/4) and (1/3, 1/3) superstructures, we evaluated the total spin-exchange interaction energies of the ordered spin structures given by the wave vector points $\Gamma$, X, M, H, and K (per $FeO_2$ layer per spin site). Our results are summarized in Table 5. In using these results, it should be recalled that $J_1 \ll J_2$, $J_3 < 0$, according to our spin dimer analysis in the previous section. Table 5 shows that the intralayer interactions $J_2$ and $J_3$ are essential for the occurrence of the (1/2, 1/4) superstructure because if $J_2 = J_3 = 0$, the four-sublattice AF structure would become degenerate with the (1/2, 0) superstructure at X and the (1/2, 1/2) superstructure at M. Furthermore, the (1/2, 1/4) superstructure can never become more stable than the (1/3, 1/3) superstructure within the scope of a Heisenberg model, because the energy difference between these two structures is determined primarily by the strongest AF interaction $J_1$ that defines the TLA.

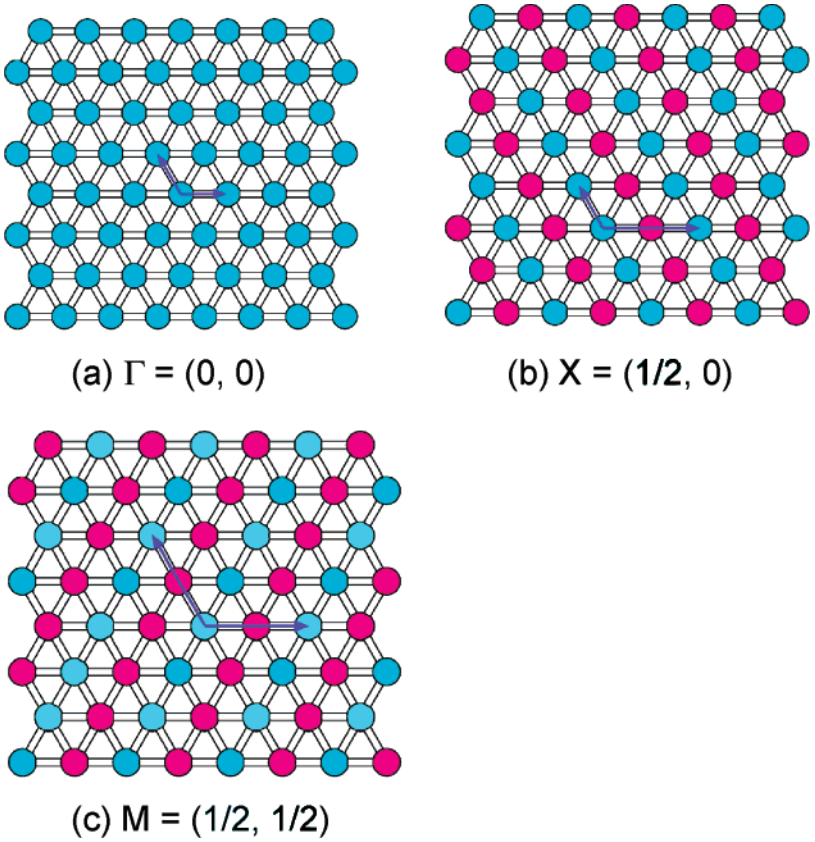


**Figure 7.** Ordered magnetic structures of an $FeO_2$ layer given by the wave vector points (a) Γ, (b) X, and (c) M.

### 4. Magnetic Moments of the Defect Ions Generated by Oxygen Nonstoichiometry

Our analyses in the previous two sections make it clear that a Heisenberg model cannot account for the occurrence of the collinear four-sublattice AF structure in $CuFeO_2$. Thus, we face a dilemma in understanding the magnetic properties of $CuFeO_2$; an Ising model is required for explaining the ordered magnetic structures below $T_{N1}$ and under a magnetic field, whereas a Heisenberg model explains the magnetic properties of $CuFeO_2$ above $T_{N1}$. This conceptual difficulty is resolved if nominally stoichiometric samples of $CuFeO_2$ contain a small quantity of point defect ions that give rise to a uniaxial magnetic moment and hence induce the surrounding $Fe^{3+}$ ions to orient their magnetic moments along the *c* axis. (It should be noted that the electrical properties of $CuFeO_2$ single crystals can be either n-type or p-type depending on the preparation methods,[24] the probable cause of which is oxygen nonstoichiometry.) The most likely defect ions present in the $CuFeO_2$ lattice would be the $Fe^{2+}$ or $Cu^{2+}$ ions resulting from oxygen nonstoichiometry.[12] In the following, we explore the plausibility of the above hypothesis.

As depicted in Figure 8a, an oxygen atom vacancy in $CuFeO_2$ generates three $FeO_5$ square pyramids. These square pyramids are only slightly different in structure from an ideal square pyramid (i.e., that resulting from an $FeO_6$ regular octahedron by removing one oxygen atom), because the $FeO_6$ octahedra of $CuFeO_2$ are almost regular in shape. For simplicity, it will be assumed that the $FeO_5$ square pyramids generated by an oxygen atom vacancy are ideal square pyramids. Our EHTB calculations show that the d-block levels of an ideal $FeO_5$ square pyramid are split as depicted in Figure 8b, where the local *z* axis is taken along the bond from the Fe to the apical O atom. Thus, as depicted in Figure 8c, the electronic ground state of an ideal $FeO_5$ square pyramid containing a high-spin $Fe^{2+}$ ($d^6$) ion is described by a linear combination of two degenerate electron configu-

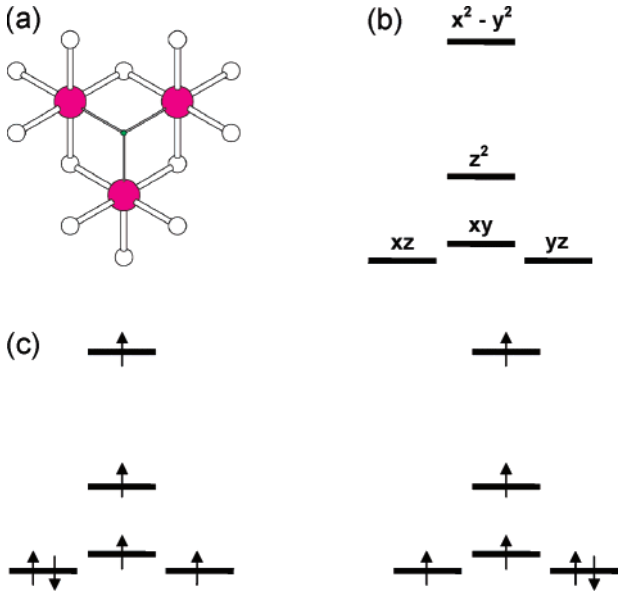


**Figure 8.** (a) Group of three $FeO_5$ square pyramids surrounding an oxygen atom vacancy (small green circle). (b) d-Block split pattern of an ideal $FeO_5$ square pyramid. (c) Two degenerate electron configurations of an ideal $FeO_5$ square pyramid containing $Fe^{2+}$.

(24) Dordor, P.; Chaminade, J.-P.; Wichanchai, A.; Marquestaut, E.; Doumerc, J.-P.; Pouchard, M.; Hagenmuller, P.; Ammar, A. *J. Solid State Chem.* **1988**, *75*, 105.

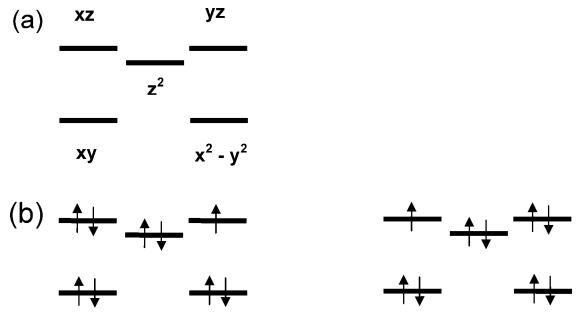


**Figure 9.** (a) d-Block split pattern of a linear O−Cu−O dumbbell. (c) Two degenerate electron configurations of a linear O−Cu−O dumbbell containing $Cu^{2+}$.

rations, where one set of degenerate orbitals (i.e., $d_{xz}$ and $d_{yz}$) has three electrons. In addition, a rotation around the 4-fold rotational axis interconverts the two orbitals. In the case of oxygen excess, some of the $Cu^{+}$ ions in the linear two-coordinate sites would be oxidized to $Cu^{2+}$ ions. Our EHTB calculations show that the d-block levels of a linear $CuO_2$ dumbbell are split as depicted in Figure 9a, where the local *z* axis is taken along the O−Cu−O axis. The $d_{z^2}$ level lies slightly lower than the $d_{xz}$ and $d_{yz}$ levels because the mixing of the Cu 4s orbital strongly reduces the sigma antibonding between the Cu $3d_{z^2}$ and the O $2p_z$ orbitals. The ground electronic state of a $CuO_2$ dumbbell containing a $Cu^{2+}$ ($d^9$) ion is described by a linear combination of two degenerate electron configurations (Figure 9b) in which one set of degenerate orbitals (i.e., $d_{xz}$ and $d_{yz}$) has three electrons, and a rotation around the O−Cu−O axis interconverts the two orbitals.

It is known [14] that a magnetic ion under a crystal field with *n*-fold ($n \geq 3$) rotational symmetry has a uniaxial magnetic moment along the *n*-fold rotational axis, if the ground state of the ion is described by a linear combination of two degenerate electron configurations in which one set of two degenerate orbitals has three electrons and if the orbitals $|L\ L_z>$ of the ion are eigenfunctions of the associated crystal-field Hamiltonian. These conditions are satisfied for the $Fe^{2+}$ and $Cu^{2+}$ ions of the $CuFeO_2$ lattice discussed above. Thus, in the case of oxygen deficiency, the $Fe^{2+}$ ion located in an ideal $FeO_5$ square pyramid should have a uniaxial magnetic moment parallel to its 4-fold rotational axis. When all three $FeO_5$ square pyramids surrounding an oxygen atom vacancy are occupied by $Fe^{2+}$ ions, the vector sum of their uniaxial magnetic moments is pointed along the *c* axis. In the case of oxygen excess, the $Cu^{2+}$ ion of a $CuO_2$ dumbbell should have a uniaxial magnetic moment along the O−Cu−O axis, i.e., along the *c* axis.

The occurrence of uniaxial magnetic moments resulting from either the $Fe^{2+}$ ions in the case of oxygen deficiency or the $Cu^{2+}$ ions in the case of oxygen excess would induce the surrounding $Fe^{3+}$ ions to orient their moments along the *c* axis, hence stabilizing the collinear four-sublattice AF structure below $T_{N1}$. It is of interest to consider implications of this hypothesis. The uniaxial magnetic moment associated with the $Fe^{2+}$ ions lies in the planes of the $Fe^{3+}$ ions, whereas that associated with the $Cu^{2+}$ ions lies outside the planes of the $Fe^{3+}$ ions. Thus, the oxygen deficiency would exert a stronger driving force for the $Fe^{3+}$ ions to orient their magnetic moments along the *c* axis than would the oxygen excess. This explains why the phase-transition temperature $T_{N2}$ is increased by oxygen deficiency ($\delta < 0$) but decreased by oxygen excess ($\delta > 0$).[12] Because the collinear four-sublattice AF structure is not observed for $CuCrO_2$,[15] one might speculate whether defect ions with uniaxial magnetic moments are absent in $CuCrO_2$. An oxygen-atom vacancy in $CuCrO_{2+}\delta$ (i.e., $\delta < 0$) would generate $Cr^{2+}$ ($d^4$) ions in $CrO_5$ square pyramids. Such a $Cr^{2+}$ ion cannot generate a uniaxial magnetic moment, because its high-spin ground-state electronic structure does not lead to a degenerate configuration according to the d-block energy levels of Figure 8b. However, the oxygen excess in $CuCrO_{2+}\delta$ (i.e., $\delta > 0$) would create $Cu^{2+}$ ions with uniaxial magnetic moments, so that the four-sublattice AF structure might be observable in such a case. The collinear four-sublattice AF structure of $CuFeO_2$ is destroyed when only 2% of the $Fe^{3+}$ ions are replaced with nonmagnetic $Al^{3+}$ ions.[18] This can be understood if the $Al^{3+}$ substitution prevents oxygen nonstoichiometry.

## 5. Concluding Remarks

Our spin dimer analysis for $CuFeO_2$ shows that the intralayer interaction $J_1$ defining a TLA is stronger than the intralayer interactions $J_2$ and $J_3$ as well as the interlayer interaction $J_4$ by a factor of approximately 30 or greater. A Heisenberg model using these spin-exchange parameters predicts that the collinear four-sublattice AF structure is less stable than the noncollinear 120° spin arrangement predicted for a TLA. Thus we examined whether defect $Fe^{2+}$ and $Cu^{2+}$ ions of the $CuFeO_2$ lattice generated by oxygen nonstoichiometry are responsible for the collinear spin alignment of the $Fe^{3+}$ ions along the *c* axis below $T_{N1}$. Our electronic structure analysis suggests that these defect ions give rise to magnetic moments pointing along the *c* axis, and hence provide a driving force for the surrounding $Fe^{3+}$ ions to orient their moments along the *c* axis below $T_{N1}$. As a consequence, an Ising model would be required for describing the magnetic structures of $CuFeO_2$ below $T_{N1}$ despite the fact that the magnetic properties of high-spin $Fe^{3+}$ ions are not uniaxial. Above $T_{N1}$, thermal agitation would negate the moment-orienting effect of the defect ions so that a Heisenberg model would be required for describing the magnetic properties of $CuFeO_2$. For nonstoichiometric $CuCrO_{2+\delta}$ samples, our hypothesis leads to the prediction that the collinear four-sublattice AF structure will be present in the case of oxygen excess ($\delta > 0$) but absent in the case of oxygen deficiency ($\delta < 0$). The presence of random point defects could also be the reason the phase transition to the collinear four-sublattice AF structure at 11 K exhibits thermal hysteresis.

**Acknowledgment.** The research was supported by the Office of Basic Energy Sciences, Division of Materials Sciences, U. S. Department of Energy, under Grant DE-FG02-86ER45259. K.-S. L. thanks The Catholic University of Korea for the 2004 Research Fund. R. K. K. thanks W. Schnelle (MPI-CPfS, Dresden) for helpful discussion.

CM052634G